

A Self-adaptive open loop architecture for weak GNSS signal tracking

Ao Peng, Gang Ou, Jianghong Shi

Abstract—An FFT-based open loop carrier tracking architecture for weak GNSS (Global Navigation Satellite System) signal is introduced in this paper, as well as a self-adaptive method which is developed to improve the stability and reliability of the architecture. Performance of the proposed architecture is analyzed theoretically. Simulation results show the proposed architecture is more stable and reliable in weak signal environments, compared with traditional close loop architecture.

Keywords—GNSS, carrier tracking, weak signal, open loop, self adaptive.

I. INTRODUCTION

THE Global Navigation Satellite System (GNSS) provides accurate positioning and timing service based on extremely accurate distance measurements from satellites to receiver. Taking GPS for instance, signal transmission time from different satellites to a specified receiver is measured through a long periodical binary pseudo-random gold code, C/A code for civilian and P(Y) code for military[1]. The receiver requires a stable carrier tracking mechanism to obtain C/A code information and navigation bits. Most traditional receivers use close-loop architectures to implement the carrier tracking architecture. They include phase lock loop (PLL), which is popular in commercial receivers for its low cost and high stability, and extended Kalman filter based tracking loop[2], which can work under lower signal-to-noise ratio environment than PLL. Many work[3-5] have been done on close-loop tracking solution to improve the loop performance by choosing appropriate integration time[3] or by using other adaptive and probabilistic methods[5]. But a drawback still exists that when the carrier-to-noise ratio (CNR) deteriorates the close-loop architectures become less stable. Once a receiver loses lock, it will take a long time to discover the loss of lock and fix it.

In comparison with close-loop architectures, open-loop architectures mainly based on FFT algorithm have a significant advantage on reliability and robustness. The carrier frequency can be directly obtained through the FFT algorithm without a

long time feed-back adjusting process, in contrast with close-loop solutions. This long time feed-back process may lead to loss of lock, especially in weak signal conditions. What's more, FFT-based open loop architecture can obtain the entire image of signal by computing the power spectrum. The signal-to-noise ratio of every observation can be derived from FFT result, with which the receiver can decide to give out valid carrier frequency estimation or make a further processing. More differences between close-loop and open-loop architectures can be seen in [6].

The main work of this paper is to develop a FFT based open loop GNSS carrier tracking architecture. The FFT calculation length in the proposed architecture is limited so that the implemental complexity is acceptable. Besides, a length-adaptive integration method is also introduced to obtain a better performance under very low CNR conditions. The rest of this paper is organized as follows: we start with the signal model in section 2. In Section 3, we present the open loop tracking architecture. The performance of the proposed architecture is then analyzed theoretically in Section 4. Simulation and analysis are performed in Section 5. Finally, conclusions are drawn in Section 6.

II. SIGNAL MODE

GPS is a Direct-Sequence code division multiple access system. Its L1C signal uses a 1.023MHz pseudo-random gold code called C/A code. The navigation data bits are BPSK modulated, and the data rate is 50Hz. The received GPS signal is down converted to intermediate frequency and sampled to a series of discrete value $s[k]$ given by

$$s[k] = Ad[k]C[k]\exp\{j[2\pi(f_{IF} + f_d)kT_s + \theta_0]\} + n_0[k] \quad (1)$$

where A is the received signal magnitude, $d[k]$ is navigation data bit, $C[k]$ is the GPS L1 C/A code, f_d is the Doppler frequency caused by relative motion between satellite and receiver, n_0 is additive white Gaussian noise with zero mean and variance σ^2 . A receiver generates two orthogonal carrier replicas and a C/A code replica. Assume C/A code has been roughly synchronized in a stable tracking case, which means the code phase difference between received signal and local replica does not exceed 1 chip length. The frequency of these two orthogonal carrier replicas is an estimated value given by the receiver, with an estimation error denoted as f_e . Here we use short time coherent

Ao Peng is with School of Information Science and Engineering, Xiamen University, Xiamen, China; (e-mail: pa@xmu.edu.cn).

Gang Ou is with School of Information Science and Engineering, Xiamen University, Xiamen, China; (corresponding author to provide e-mail: ougang@xmu.edu.cn).

Jianghong Shi is with School of Information Science and Engineering, Xiamen University, Xiamen, China; (e-mail: shijh@xmu.edu.cn).

integration to improve the SNR. The coherent integration time is an integer multiple of 1ms, which is the period of C/A code.

Figure 1 shows the scheme of signal pre-processing, where sampled GPS signal is multiplied by two orthogonal carrier replicas and then de-spread and integrated to improve the SNR. The pre-processed result can be expressed as follows

$$r_i[k] = Ad[k]R(\Delta)\text{Sinc}(f_e T_i) \exp[j2\pi f_e k T_i + \theta_e] + n'[k] \quad (2)$$

where T_i is the number of coherent integrated samples. $R(\Delta)$ is correlation function of C/A code, Δ is the code phase difference

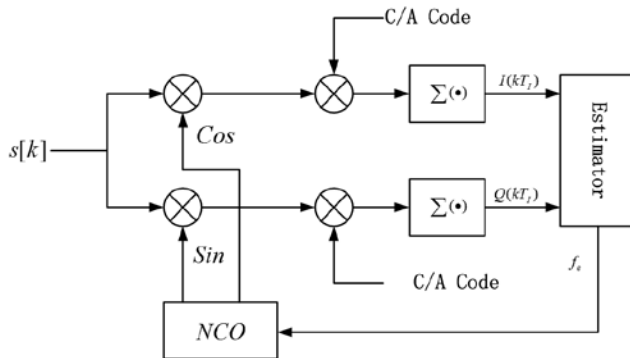


Fig. 1 Scheme of pre-processing

between received signal and local C/A code replica, $n'[k]$ is a complex Gaussian noise characterized by zero mean and σ^2/T_i variance [7].

When code phase difference is greater than 1 chip, the value of C/A code correlation function approaches zero. $R(\Delta)$ shows the effect of code phase estimation error on carrier frequency estimation. $\text{Sinc}(x)$ denotes the integration loss caused by frequency error. The pre-process result can also be simply written as

$$r_i[k] = A'd[k] \exp(\theta_e) \exp(j2\pi f_e k T_i) + n'[k] \quad (3)$$

where $A' = AR(\Delta)\text{Sinc}(f_e T_i)$, $n'[kT_i] \sim N(0, \sigma^2/T_i)$.

During the processing period, frequency error f_e and code phase error $\Delta\tau$ can be treated as constants, so the modified signal magnitude A' is also a constant.

As we can see, $r_i[k]$ has a single frequency spectrum with sampling period T_i . In traditional GPS receivers, a phase discriminator is always used to get a valid measurement on $r_i[k]$. Taking optimal arctangent discriminator as an example, as signal power goes weaker, its noise performance deteriorate nonlinearly[3]. What's more, traditional phase discriminators do not tell the reliability of its outputs because they only provide noise-mixed observation results. On the contrary, Fourier Transform provides another way to achieve frequency observation and its reliability. Fourier transform calculates power on all sampled frequencies, including frequency with signal and frequencies without signal. So for every observation, reliability measurement can be easily made by comparing the signal power to noise power. Thus, further processing decision can be made based on the reliability.

In (3), the duration of navigation data bit $d[k]$ is 20ms. The effect caused by data bit transitions should be removed when more than one data bit duration is involved in tracking process. In [2, 8, 9], different methods of real-time navigation data bits estimation are reported. The navigation data bits can also be obtained from a nearby reference station. Therefore, $d[k]$ is considered as known in the following parts.

In the following part of this paper, an open loop and self-adaptive integration method basing on FFT algorithm will be developed to give a reliable and stable estimation on f_e .

III. OPEN LOOP TRACKING ARCHITECTURE

Fourier transform is widely used in signal acquisition [10], and until now there are some works [6, 11] using it in GPS signal tracking. In comparison with close-loop tracking architectures such as PLL or EKF-based tracking loop, FFT-based architecture needs large storage resource, arithmetic resource and long calculation period. However, FFT-based architecture has some aspects which are really attractive to carrier tracking. First, Fourier transform gives an overview of signal spectrum and GPS signal, after de-spreading, is a single frequency signal, which means there should be only one peak in the Fourier transform result. So the observation reliability is inherently included in the Fourier transform result. Second, in each calculation period Fourier transform only need current data samples, and history results have no effect on the current result. So its shock response rate is much higher than loops. Third, FFT-based tracking architecture do not need additional lock-loss detector. Due to such advantages, a FFT-based open loop tracking architecture is proposed in this paper.

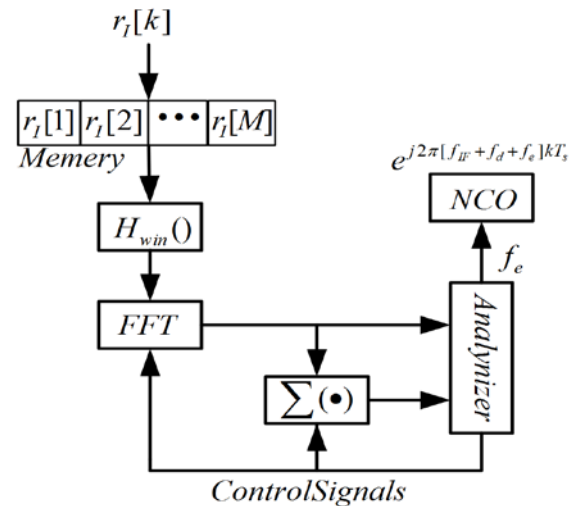


Fig. 2 Block diagram of FFT-based open loop tracking architecture

Fig. 2 shows the block diagram of FFT-based Open loop tracking architecture. The pre-processed samples $r_i[k]$ are stored in a buffer and truncated into groups. Length of these groups is equal to the FFT length. A 32-point or 64-point FFT is used here. FFT length decides frequency resolution when the sampling frequency keeps constant. In the pre-processing

module the coherent integration time is T_I , and if FFT length is L , frequency resolution can be expressed by

$$\Delta f = \frac{1}{LT_I} \quad (4)$$

Spectral leakage caused by discrete Fourier transform results in attenuation on SNR, so a window function $h_{win}^{(L)}$ is used to reduce the spectral leakage. The Fourier transform of $h_{win}^{(L)}$ is denoted as $H_{win}(\omega)$. There are 2 important factors to be considered when choosing a proper window function: main lobe width and side lobe suppression ratio (SLSR). Because $r_i[k]$ is a narrowband signal, so SLSR is much more important than main lobe width. One effective method to suppress the side lobe is using the Hanning window. The first side lobe attenuation of Hanning window is -32dB while the rectangle window has only 13dB attenuation on the first side lobe. The FFT result is

$$Y_I(k) = \sum_{l=0}^{L-1} r_I(l) h_{win}(l) \exp\left(\frac{-j2\pi kl}{L}\right) \quad (5)$$

where $h_{win}(l)$ is Hanning window

$$h_{win}(l) = 0.5 - 0.5 \cos\left(\frac{2\pi l}{L}\right) \quad (6)$$

By taking (3) in to (5), we get

$$Y_I(k) = A' H_{win}(k) \exp\left[j\pi f_\varepsilon (L-1)\right] \frac{\sin(\pi L f_\varepsilon)}{\sin(\pi f_\varepsilon)} \quad (7)$$

When $f_\varepsilon = f_e T_I - k/L \approx 0$, $|Y_I(k)|$ meets its maximum value.

Frequency error can then be derived as

$$f_e = \frac{k}{LT_I} + \varepsilon \quad (8)$$

where ε shows the discrete property of FFT, that FFT cannot make an accuracy estimation and there is always a frequency quantization error. The value of quantization error does not exceed half of frequency resolution

$$|\varepsilon| \leq \frac{1}{2LT_I} \quad (9)$$

As shown in Fig. 2, there is an accumulation bypass denoted by $\sum(\cdot)$. The accumulation operation is defined as

$$S_{xx}(k) = \frac{1}{M} \sum_{i=0}^{M-1} |Y_I(i, k)|^2 \quad (10)$$

where M is accumulation period which is decided dynamically by the succeeding analyzer, and $Y_I(i, k)$ denotes the FFT result on the k th sampling frequency in calculation period i . It's obvious that the accumulation bypass provides power spectrum estimation on $r_i[k]$. Due to accumulation operation, the SNR of power spectrum estimation can be reduced by a factor of M [12, 13]. Accumulation bypass is controlled by the analyzer, both on integration operation and clearing operation.

The main function of analyzer shown in Fig. 2 is evaluating the reliability of FFT result and accumulation result from the bypass based on SNR. Here SNR is defined by

$$SNR = \max \left\{ \frac{|Y_I(k)|_{\max}^2}{|Y_I(k)|_{2ndPeak}^2}, \frac{|S_{xx}(k)|_{\max}^2}{|S_{xx}(k)|_{2ndPeak}^2} \right\} \quad (11)$$

where $|Y_I(k)|_{\max}$ is the max peak value of FFT result $|Y_I(k)|$, and $|Y_I(k)|_{2ndPeak}$ is the second max peak value of $|Y_I(k)|$; $|S_{xx}(k)|_{\max}$ is the max peak value of accumulation result $|S_{xx}(k)|$ and $|S_{xx}(k)|_{2ndPeak}$ is the second max peak value of $|S_{xx}(k)|$. A threshold TH_{SNR} is used here to filter bad estimations. New estimation is not available until SNR is greater than TH_{SNR} .

Another function of the analyzer is to generate control signals to FFT module and accumulation bypass. These control signals are classified into 3 states, as described in the following.

1. Fast calculation. In this state, 32-point FFT is used, and the accumulation bypass clears its history result at the beginning of the current period. This is the basic state of the open loop tracking architecture. When SNR is greater than the threshold, which means a new estimation was available in the previous period, the historic accumulation result is cleared and a new accumulation period begins.

2. Accumulation. In this state, 32-point FFT is used, and the accumulation bypass is working. This state happens in the case that SNR in the previous period was smaller than the threshold. In this state no reliable estimation is obtained so NCO keeps its oscillation frequency.

3. Fine calculation. In this state, 64-point FFT is used, and the accumulation bypass stops working. This state is designed to increase the reliability of the frequency estimation which is analyzed in the next part. When tracking is stable, which is defined by more than 5 continuous Fast calculation periods, FFT length spreads to 64 points. Current state does not change from Fine calculation into Fast calculation until SNR is not greater than threshold.

Working state switches automatically among these 3 states. Therefore, this open loop tracking architecture is self-adaptive to the dynamic environment.

In the following part, performance of the above proposed architecture is analyzed theoretically.

IV. PERFORMANCE ANALYSIS

Frequency error estimation is derived from (8), where k denotes the index of maximum peak value. By taking (8) into (7), the expression of max peak value is obtained by

$$\max\{|Y_I(k)|\} \approx A' L H_{win}(k) \text{Sinc}(\pi L \varepsilon) \quad (12)$$

where the approximation $\sin(\pi \varepsilon) \approx \pi \varepsilon$ is adopted, and the noise is not taken into consideration. In (2), $n[k] = n'_i[k] + jn'_o[k]$, where $n'_i[k]$ and $n'_o[k]$ are both independent Gaussian White Noise with distribution of

$$\{n'_i, n'_o\} \sim N\left(0, \frac{\sigma^2}{2T_I}\right) \quad (13)$$

so the FFT results of $n[k]$ is

$$N'(k) = \sum_{l=0}^{L-1} \left\{ [n'_I(l) + jn'_Q(l)] h_{win}(l) \exp\left(-j \frac{2\pi}{L} kl\right) \right\} \quad (14)$$

Since $n'_I(l)$ and $n'_Q(l)$ ($l=0, 1, \dots, L-1$) are independent Gaussian random variables, the linear combinations of them are also Gaussian random variables. Divide (14) into real part and imaginary part

$$N'_{Re}(k) = \sum_{l=0}^{L-1} \{n'_I(l) \cos \omega_{l,k} + n'_Q(l) \sin \omega_{l,k}\} h_{win}(l) \quad (15)$$

$$N'_{Im}(k) = \sum_{l=0}^{L-1} \{-n'_I(l) \sin \omega_{l,k} - n'_Q(l) \cos \omega_{l,k}\} h_{win}(l) \quad (16)$$

where $\omega_{l,k} = 2\pi lk/L$. Both $Re[N'(k)]$ and $Im[N'(k)]$ are zero-mean Gaussian random variables, and their variances are [14]

$$Var\{N'_{Re}(k)\} = Var\{N'_{Im}(k)\} = \frac{L\sigma^2 H_{win}^2(k)}{T_I} \quad (17)$$

The power spectrum of noise obeys exponential distribution with rate parameter $1/LT_I\sigma^2 H_{win}(k)$. The possibility density function (PDF) of noise power spectrum is

$$f(x) = \frac{T_I}{L\sigma^2 H_{win}(k)} \exp\left[-\frac{T_I}{L\sigma^2 H_{win}(k)} x\right] \quad (18)$$

When noise is ignored, the result of (12) is deterministic. When taking noise into consideration, FFT result on the main peak

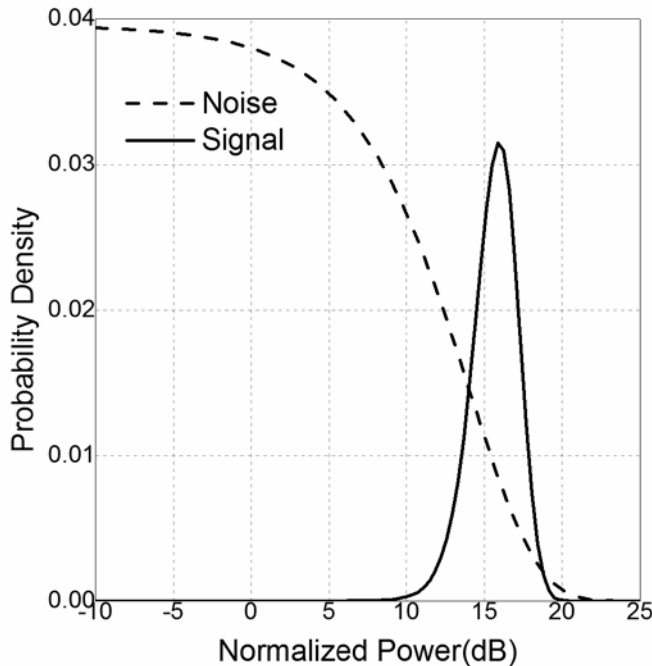


Fig. 3 Probability distribution of power spectrum (CNR=15dB-Hz)

frequency becomes a complex Gaussian random variable, whose mean is $Y_I[k]$ and variance is $Var[N'(k)]$. Let $P[Y_I(k)]$ denotes the power of signal without noise, we have

$$P_{max} = P[Y_I(k)]_{max} + Var[N'(k)] \approx [A' L H_{win}(k) Sinc(\pi L \varepsilon)]^2 + \frac{L H_{win}^2(k) \sigma^2}{T_I} \quad (19)$$

The power on the main peak obeys non-central Chi-squared distribution with degree of freedom $\nu=2$. So its PDF is [15]

$$g(x) = \frac{1}{2} \exp\left(-\frac{x+\lambda}{2}\right) I_0(\sqrt{\lambda x}) \quad (20)$$

where λ is defined by

$$\lambda = \left[\frac{A' T_I L Sinc(\pi L \varepsilon)}{\sigma} \right]^2 \quad (21)$$

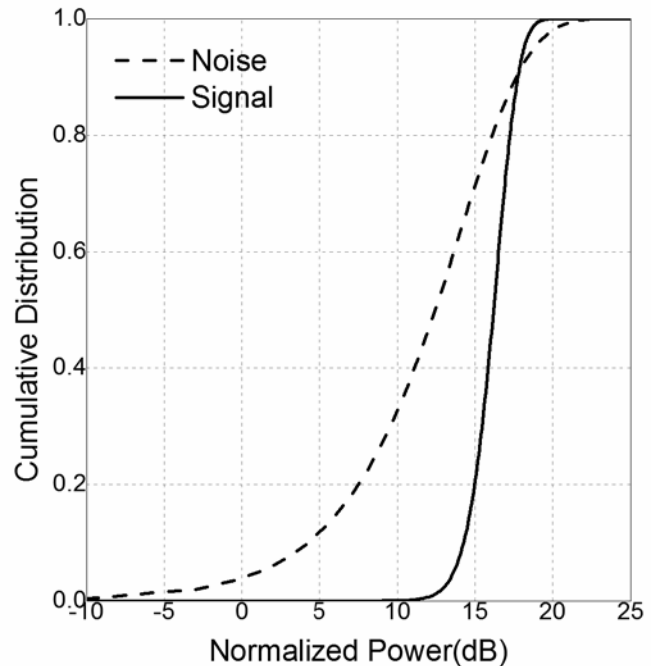
and $I_0(x)$ is zero order modified Bessel function of the first kind.

The cumulative distribution functions (CDF) of $f(x)$ and $g(x)$ are denoted by $F(x)$ and $G(x)$ respectively. We have

$$F(x) = \int_{t=0}^x f(t) dt = 1 - \exp\left[-\frac{T_I x}{L\sigma^2 H_{win}(k)}\right] \quad (22)$$

$$G(x) = \int_{t=0}^x g(t) dt \quad (23)$$

Fig. 3 shows an example of probability distribution. The received satellite signal power in (1) is assumed to be normalized, and the carrier-to-noise ratio (CNR) is 15dB-Hz. It also assumes ideal code tracking, so that attenuation $R(\Delta)$



caused by code phase error can be ignored. The left part of Fig. 3 shows CDF, while PDF is shown in the right part. It can be seen that the probability is almost the same when the noise power level is no more than 5dB, and the noise power level has a high likelihood (>0.7) to stay below 15dB. On the contrary, there is a high probability (>0.9) that the signal power lies between 15dB and 20dB.

Equation (3) shows that the GPS signal is a single frequency signal after de-spreading. So after Fourier transform, signal only exists on the corresponding frequency, while the rest power spectrum can be considered as noise spectrum. Denote frequency index with signal by k_s , the FFT results obey the following distribution

$$\Pr\{|Y_i(k)|^2 < x\} = \begin{cases} G(x); k = k_s \\ F(x); k \neq k_s \end{cases} \quad (24)$$

In the Fast calculation state and Fine calculation state, valid frequency estimation is obtained when the current SNR is greater than the threshold, with peak value P_{max} . Denote the event “The main peak appears on i th frequency with peak value P_{max} and all other power values are smaller than P_{max} / TH_{SNR} ” by E_i , then the probability of E_i is

$$\Pr\{E_i\} = \begin{cases} g(P_{max}) \prod_{k \neq k_s} F\left(\frac{P_{max}}{TH_{SNR}}\right); i = k_s \\ f(P_{max}) G\left(\frac{P_{max}}{TH_{SNR}}\right) \prod_{k \neq k_s, k \neq i} F\left(\frac{P_{max}}{TH_{SNR}}\right); i \neq k_s \end{cases} \quad (25)$$

A correct estimation is obtained only when E_i happens and $i = k_s$. The error rate can then be derived by

$$P_e = \Pr\{i \neq k_s | E_i\} = 1 - \frac{\Pr\{E_{k_s}\}}{\sum_L \Pr\{E_i\}} \quad (26)$$

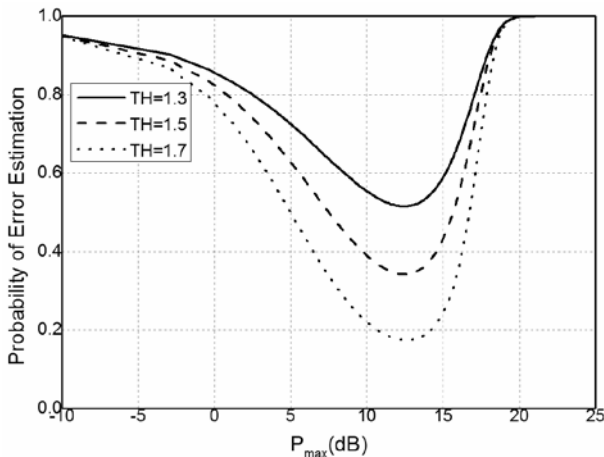


Fig. 4 Probability of error estimation vs. Pmax

Different thresholds are compared in Fig. 4. The CNR is 15dB-Hz. When P_{max} locates in the area between 10dB and 15dB, the rate of error estimation is relatively low. Referring to the PDF shown in Fig. 3, signal power has a big probability to locate in this area. Fig. 4 also shows that probability of error estimation decreases if the threshold increases. If the threshold is set to be 1.7, the probability of error estimation is less than 0.2. However, increasing the threshold means the noise power stays at a lower level, which equals to the decrease of the probability of E_i . A valid estimation can't be obtained if E_i doesn't happens. Such a tradeoff should be considered when choosing the value of the threshold

In the Accumulation state, the average of power spectra in accumulation period is taken as the estimated power spectrum. The accumulation process will not stop until SNR is greater than the threshold. The average action leads to reduction of noise variance. There are M segments referring to (10), so the variance is reduced by M [12]. The relationship between M and error estimation probability is shown in Fig. 5, where a threshold of 1.3 is used and CNR is 13dB-Hz. As we can see in Fig. 5, the minimal error estimation probability is greater than 0.75 when no accumulation taken place ($M=1$). However when the accumulation state lasts for 3 period ($M=3$), the error probability decreases to around 0.05 when P_{max} is between 15dB and 20dB. After accumulation, the reliability of estimation is improved significantly.

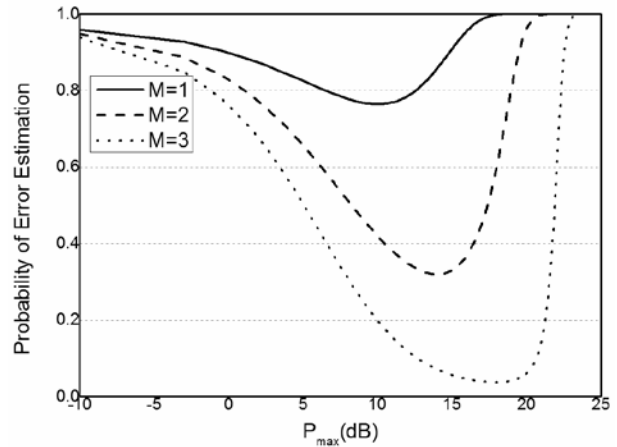


Fig. 5 Probability of error estimation under different accumulation lengths

In Fine calculation state, 32-point FFT is replaced by 64-point FFT. The changes are shown in Fig. 6, where CNR is 15dB-Hz and the threshold is 1.3. The left part shows the difference in PDFs. The typical area of signal power with high probability rises from 13~18dB to 17~21dB. The difference in estimation reliability is shown in the right part. When using 64-point FFT, the minimal probability of error estimation decreases from 0.5 to 0.22.

V. SIMULATION RESULTS

In this section, performance of the proposed open loop tracking architecture based on FFT algorithm under weak signal environments is validated by simulations. To focus on the carrier tracking performance, ideal code tracking is assumed. The Doppler frequency is modeled as changing linearly over time, with a fix but noise affected Doppler rate. The initial frequency error is -50Hz, which is guaranteed by the precision of the acquisition module. The fixed Doppler rate is set to be -0.5Hz/sec, and the noise added to the Doppler rate is Gaussian white noise with zero mean and unit variance.

Sampling frequency of the received satellite signal is 16.367MHz, and the coherent integration time is 0.005sec. Therefore the number of coherent integration samples is 81838.

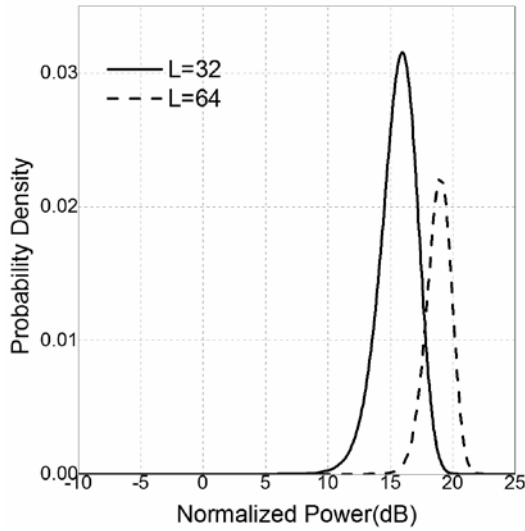


Fig. 6 Differences between fast calculation state and fine calculation state

Cases with different CNRs are tested and errors of frequency estimation are shown in Fig. 7. In Figs 7(a), 7(b) and 7(c), the CNRs are 13dB-Hz, 14dB-Hz and 15dB-Hz respectively. In Fig. 7(a), it takes a long time to achieve stable tracking state. In Fig. 7(b), a big estimation error happens around 47sec, and the tracking state quickly recovers in the next update period. In Fig. 7(c), when the CNR is 15dB-Hz, there is no big estimation error among the test period, and at most part of the period the estimation error is within +/-5Hz. In all the 3 test cases the proposed architecture keeps tracking to the Doppler frequency, and no lock-loss happens during 70 seconds. It can be concluded that the open loop tracking architecture based on FFT algorithm is stable and reliable under weak signal environments.

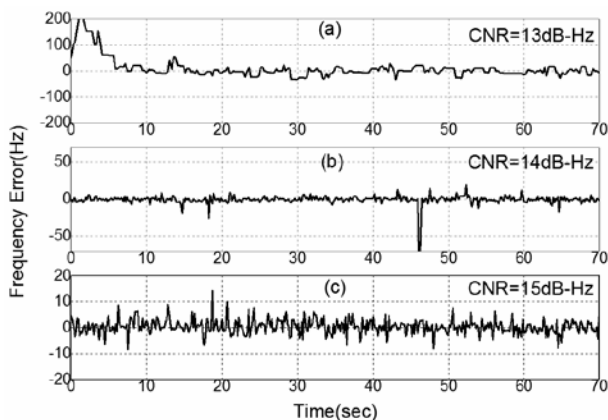
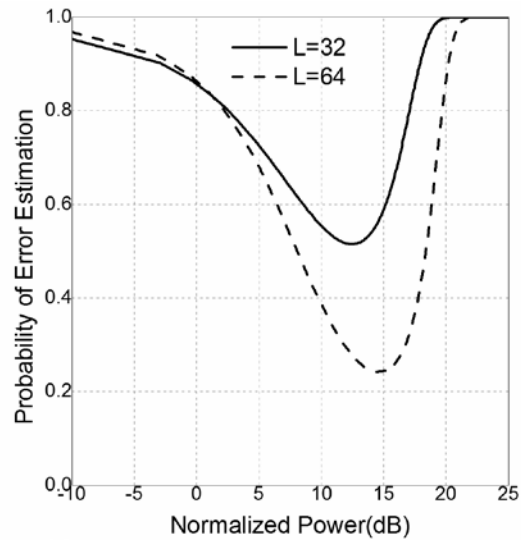


Fig. 7 Performance under different CNRs

The proposed architecture is also compared with classical close loop architecture based on extended Kalman filtering. The details of an EKF based carrier tracking loop can be found in [2, 8]. The coherent integration period of the EKF based loop is set to be 5ms, the same as it used in the proposed open loop architecture. And the non-coherent length of the EKF based

loop is 32. To validate the tracking ability under weak signal environments, the simulation is setup as follows. At the beginning of the simulation, the CNR is 33dB-Hz. It decreases



by 4dB-Hz every 100 seconds until 13dB-Hz. The CNR remains 13dB-Hz for 200 seconds and then rises with a speed of 4dB-Hz per 100 seconds. A simple CNR estimator is used as lock indicator. The results are shown in Fig.8. For the proposed open loop architecture, the estimated CNR fluctuates heavily when the truth value drops to 13dB-Hz. However, it still keeps tracking to the carrier. When the CNR rises up again, the variation trends of the estimated CNR is same to the truth value. For the compared EKF based architecture, loss of lock happens when CNR drops to 13dB-Hz. The estimated CNR decreases to 0 as shown in Fig.8, which means no signal power is detected. And when the CNR rises up again, the estimated CNR was not recovered.

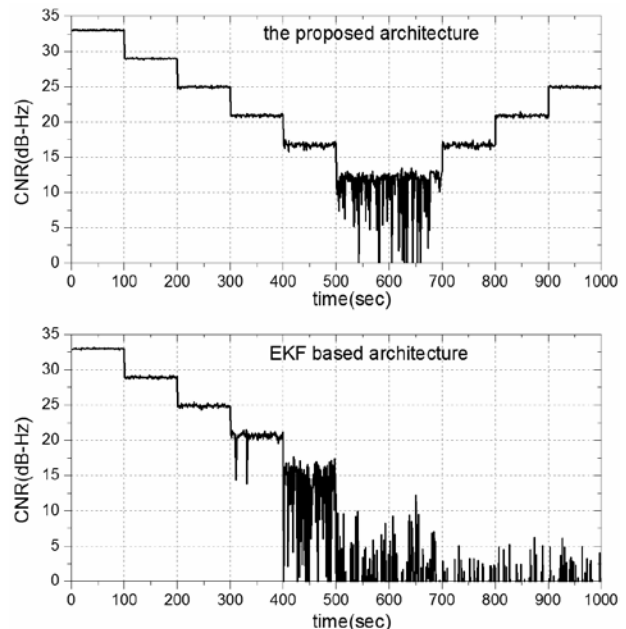


Fig. 8 Comparison with the classical close loop architecture

The self-adaptive property of this open loop architecture is tested by statistics of time spent in the 3 different tracking state, fast calculation, accumulation and fine calculation. It's shown in Fig. 9. When the CNR is 15dB-Hz, the proposed architecture is working in Fine calculation state most of the time. As noise power rising, the architecture needs more time for accumulation. When the CNR decreases to 13dB-Hz, rare time is spent in Fine calculation state, and the working state switches between Accumulation and Fast calculation to obtain a stable condition.

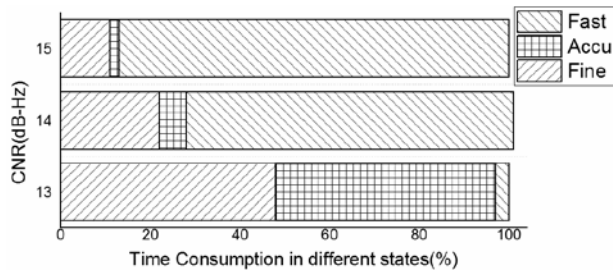


Fig. 9 Time statistics in different states

VI. CONCLUSIONS

An FFT based open loop carrier tracking architecture for GNSS signals under weak signal conditions is proposed. The proposed architecture works reliable for that it can inspect the reliability of estimation value by computing the instantaneous SNR. Moreover, the architecture is self adaptive to the environment because it can adjust the average length of power spectrum during the accumulation state automatically. By adjusting the average length, the reliability of the frequency error estimation improves significantly. Due to the time independent property of the Fourier transform, once a significant estimation error happens, the architecture can quickly restore to the stable tracking state. Simulation shows that the architecture can maintain a stable carrier tracking with CNR as low as 13dB-Hz. We therefore argue that for weak signal applications of GNSS, open loop architecture may be a good choice in comparison with the traditional close loop architecture.

REFERENCES

- [1] J. Spilker Jr, "GPS signal structure and performance characteristics," *Navigation*, vol. 25, pp. 121-146, 1978.
- [2] M. L. Psiaki and H. Jung, "Extended Kalman filter methods for tracking weak GPS signals," 2001, pp. 2539-2553.
- [3] C. O'Driscoll, M. G. Petovello, and G. Lachapelle, "Choosing the coherent integration time for Kalman filter-based carrier-phase tracking of GNSS signals," *GPS solutions*, pp. 1-12, 2011.
- [4] A. Razavi, D. Gebre-Egziabher, and D. M. Akos, "Carrier loop architectures for tracking weak GPS signals," *Aerospace and Electronic Systems, IEEE Transactions on*, vol. 44, pp. 697-710, 2008.
- [5] D. J. Jwo and S. H. Wang, "Adaptive fuzzy strong tracking extended Kalman filtering for GPS navigation," *Sensors Journal, IEEE*, vol. 7, pp. 778-789, 2007.
- [6] F. van Graas, A. Soloviev, M. Uijt de Haag, and S. Gunawardena, "Closed-Loop Sequential Signal Processing and Open-Loop Batch Processing Approaches for GNSS Receiver Design," *Selected Topics in Signal Processing, IEEE Journal of*, vol. 3, pp. 571-586, 2009.

- [7] A. Van Dierendonck, P. Fenton, and T. Ford, "Theory and performance of narrow correlator spacing in a GPS receiver," *Navigation*, vol. 39, pp. 265-283, 1992.
- [8] N. Ziedan and J. Garrison, "Bit synchronization and Doppler frequency removal at very low carrier to noise ratio using a combination of the Viterbi algorithm with an extended Kalman filter," 2001, pp. 616-627.
- [9] A. Soloviev, F. Van Graas, and S. Gunawardena, "Decoding navigation data messages from weak GPS signals," *Aerospace and Electronic Systems, IEEE Transactions on*, vol. 45, pp. 660-666, 2009.
- [10] D. Akopian, "Fast FFT based GPS satellite acquisition methods," 2005, pp. 277-286.
- [11] S. Satyanarayana, D. Borio., and G. Lachapelle, "A Non-Coherent Block Processing Architecture for Standalone GNSS Weak Signal Tracking," in *ION GNSS 2011*, Portland, OR, 2011.
- [12] K. Barbé, R. Pintelon, and J. Schoukens, "Welch method revisited: nonparametric power spectrum estimation via circular overlap," *Signal Processing, IEEE Transactions on*, vol. 58, pp. 553-565, 2010.
- [13] J. G. Proakis and D. G. Manolakis, "Digital signal processing: principles, algorithms, and applications," 1992.
- [14] Q. Liu and Z. Li, "The statistic property and applications of Gaussian white noise sequence spectrum," *Acoustics and Electronics Engineering*, vol. 1, 2003.
- [15] J. Marcum, "A statistical theory of target detection by pulsed radar," *Information Theory, IRE Transactions on*, vol. 6, pp. 59-267, 1960.